PHYSICAL REVIEW E **85**, 050601(R) (2012)

# Dimensional crossover in fluids under nanometer-scale confinement

Amit Das* and J. Chakrabarti†

*Department of Chemical, Biological and Macromolecular Sciences, S. N. Bose National Centre for Basic Sciences, Block JD, Sector III, Salt Lake, Kolkata-700 098, India*

(Received 26 November 2011; revised manuscript received 27 March 2012; published 10 May 2012)

Several earlier studies have shown signatures of crossover in various static and dynamics properties of a confined fluid when the confining dimension decreases to about a nanometer. The density fluctuations govern the majority of such properties of a fluid. Here, we illustrate the crossover in density fluctuation in a confined fluid, to provide a generic understanding of confinement-induced crossover of fluid properties, using computer simulations. The crossover can be understood as a manifestation of changes in the long-wavelength behavior of fluctuation in density due to geometrical constraints. We further show that the confining potential significantly affects the crossover behavior.

DOI: 10.1103/PhysRevE.85.050601 PACS number(s): 68.15.+e

Fluids under confinement represent a very important class of system relevant in various branches of science and technology, from biology [1] to tribology [2]. A bulk three-dimensional (3D) fluid is expected to behave as a two-dimensional (2D) system when confined to length scale, comparable to molecular size. Consequently, when a fluid is kept in an enclosed space, many of its behaviors alter dramatically [3]. The understanding of crossover in fluid properties from 3D to 2D behavior is one of the most challenging problems, having both scientific and technological importance. In reality, this crossover takes place in the presence of a confining potential which makes the situation even more interesting.

Confined water has drawn considerable attention in the recent past: Surface force measurements show that water molecules confined to a film of three to four molecular diameters (∼a nm) thickness, undergo ordering similar to a solid [4]. The mechanical relaxation time ($\tau$) to dissipate the stress after an external strain is applied becomes almost an order of magnitude larger compared to the corresponding bulk value under a confinement less than a nanometer. Such changes have also been observed under nanometer scale confinements in other molecular properties which depend on the collective response of the system. The melting temperature of water drops significantly when confined in silica nanopores of diameter ∼3 nm as revealed by Raman scattering measurements [5]. Water confined in reverse micelles of a diameter ∼nm [6] has a static dielectric constant ($\varepsilon_0$) that is three to four times lower than the bulk value (∼80) [7]. Sudden jumps in the viscosity ($\eta$) and diffusivity ($D$) have been observed [8] in the case of linear alkanes and alcohols in organosilicate nanopores of a diameter of less than 2 nm. Measurements of refractive index ($n$) and the equilibrium film thickness of cyclohexane confined within two mica plates have shown a sudden transition from a 3D bulk fluid to a 2D adsorbate for plate separation around a couple of nanometers, with significant enhancement in fluctuations of refractive index, changes in phase-transition temperatures and normalized enthalpies, lowering of critical temperature, and anomalous fast self-diffusion [9]. However, such changes in fluid properties under confinement depend on the nature of the confining potential. Reference [10] studies water in subnanometer confinements where the viscosity increases substantially in a hydrophilic environment but not having so much of an effect in a hydrophobic confinement.

There have been a number of theoretical studies on confinement induced effects. Reference [11] reports on an extensive grand-canonical Monte Carlo (GCMC) simulation [12] to calculate the static properties of confined fluid and shows their sensitivity to the wall structure. Reference [13] derives the weighted density functional theory of a 2D fluid as a limiting case of the corresponding functional for an inhomogeneous 3D fluid within a linearized approximation. Several other theoretical and simulation studies address various problems related to confinement such as capillary condensation [14], adsorption on solid surfaces [15], freezing behavior [16], dynamic properties such as the in-plane diffusion coefficient [17,18] and rotational correlation time [18] and the glass transition [19]. The 3D to 2D crossover under confinement has been studied extensively near the critical point [20–22]. However, the question how the confinement-induced crossover takes place in various fluid properties away from a critical point has remained largely unaddressed.

The wave vector ($k$) dependent fluctuations in density govern the majority of properties of a fluid, including static quantities such as dielectric constant and refractive index, as well as long-time dynamic quantities such as viscosity and the self-diffusion coefficient and so forth [23]. Hence, the crossover in all such properties should be generically related to that in density fluctuations. We calculate to this end the fluctuation in number of particles $N$ in a slit of parallel walls with a fixed volume $V$ at absolute temperature $T$, $\Delta = \langle (N - \langle N \rangle)^2 \rangle / \langle N \rangle$, the angular brackets representing ensemble averages generated by GCMC simulations [12,24], where the confined fluid is maintained at a chemical potential $\mu$ that is the same as that of the bulk far away from any phase-transition point. The generality of experimentally observed crossover, independent of system specific details, leads us to consider a model fluid with a model wall-fluid potential to capture qualitatively the generic effect of confinement. We show that $\Delta$ undergoes a crossover from 3D to 2D behavior without any accompanying phase transition below

*amitsearch@bose.res.in
†jaydeb@bose.res.in

 

a confinement extending only a few molecular diameters, measuring about a nanometer, the same length scale of crossover observed in the experiments. Further, the crossover in $\Delta$ can be understood from the suppression of the density fluctuations in the system in a direction perpendicular to the slit, beyond the wavelength given by the length scale of the confinement. The dynamic density fluctuations, given in terms of the Van Hove correlation function (VHCF), computed from molecular dynamics (MD) simulations in an *NVE* ensemble ($E$, total energy) [25] with initial conditions chosen from the GCMC configurations [26], also exhibit similar crossover in the in-plane diffusivity $D_{\parallel}$. However, the crossover is dependent on the confining potential: 3D to 2D crossover in $\Delta$ and $D_{\parallel}$ for a fluid in a solvophobic slit is significantly different from that in a solvophilic pore due to strong layering of the fluid particles near the wall by a large wall attraction in the latter case. We relate our observations to experimental observations on different fluid properties that are dependent on density fluctuations.

The model fluid is taken in a rectangular simulation box with two parallel slits placed at a separation $H$ on the $z$ axis at $z = -H/2$ and $z = H/2$, with fixed box lengths along the $x$ and $y$ axes ($L_x = L_y = 20\sigma$, $\sigma$ being the particle diameter). Here, the periodic boundary conditions are applied along the $x$ and $y$ directions only. We consider a truncated Lennard-Jones (LJ) potential with a cutoff radius $L_x/2$ as the interparticle interaction, $u(r) = 4\varepsilon[(\sigma/r)^{12} - (\sigma/r)^6]$, $\varepsilon$ being the interaction strength and $r$ the interparticle separation. Due to large cutoff we have not added any corrections due to truncation. The confining potential type is varied: hard walls only reflecting the colliding particles, repulsive walls with a wall-fluid interaction for a particle at $z$, $u_{w-f}(z - H/2) = 4\varepsilon'(\sigma/|z - H/2|)^{10}$, and attractive walls, $u_{w-f}(z - H/2) = 4\varepsilon'[(\sigma/|z - H/2|)^9 - (\sigma/|z - H/2|)^3]$, where $\varepsilon' = 10\varepsilon$. The simulations have been performed at a LJ temperature $T^*(= k_BT/\varepsilon) = 2.0$ with a chemical potential [12] $\mu^*(= \mu/k_BT) = 0.4$, far away from any phase-transition point [27]. In the MD simulations, we use the Verlet algorithm [12] to integrate the equations of motion with a time step of 0.005 LJ units [$\tau_0 = (m\sigma^2/\varepsilon)^{1/2} \sim 2.8 \times 10^{-12}$ s for argon, where $m$ is the mass of argon atom] [25]. The self parts of an in-plane VHCF [19], $G_s(r_{\parallel},t) = (1/N)\langle\sum_i \delta(\vec{r}_{\parallel} - \vec{r}^{\,i}_{\parallel}(0) + \vec{r}^{\,i}_{\parallel}(t))\rangle$, are computed where $\vec{r}_{\parallel}$ is the space variable parallel to the walls (along the $x$-$y$ plane) and $\vec{r}^{\,i}_{\parallel}(t)$ is the position of the $i$th particle along the $x$-$y$ plane at time $t$. In the long time limit, the VHCF is Gaussian, $G_s(r_{\parallel},t) \approx (1/4\pi D_{\parallel}t)\exp[-r_{\parallel}^2/4D_{\parallel}t]$.

The fluid density profiles in the direction normal to the slits ($z$ axis), given by the number of particles in a particular fluid segment of width $\sim 0.1\sigma$, exhibit layering for different wall types similar to those in earlier studies [10,11,13]. Structurally, the wall-adjacent layers for any type of wall assume 2D behavior, as suggested by the in-plane radial distribution function (RDF) [11,28,29]. For reflecting walls, at $H = 4\sigma$, the central region is a fluid segment of one diameter width, the corresponding RDF revealing a 2D structure. For $H > 4\sigma$, the central region of uniform density appears, revealing a 3D bulklike RDF, which gets extended as confinement is relaxed. These features of the central region are qualitatively the same for the other wall types as well. The well-formed central region resembles the bulklike inner core of water inside large reverse micelles [30]. The other layers formed in between the central region and the wall-adjacent layers behave quite similarly as a 2D fluid.

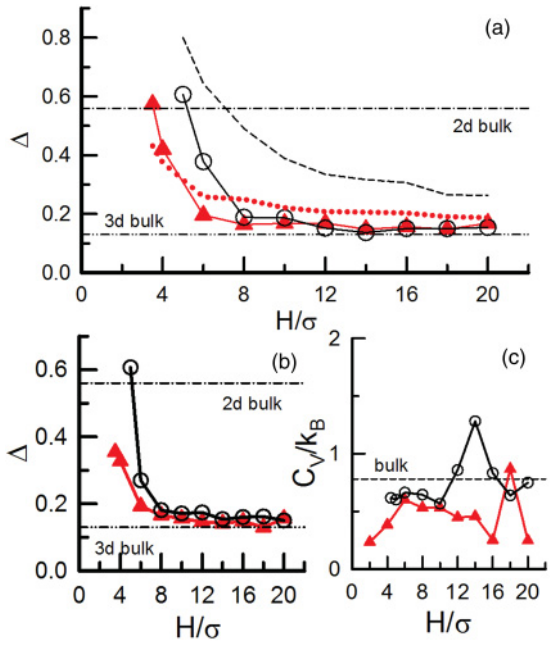


FIG. 1. (Color online) Different quantities in slits as functions of $H$: (a) $\Delta$, reflecting (triangles: simulation; dotted line: theory) and repulsive (circles: simulation; dashed line: theory); (b) $\Delta$ in the central region, reflecting (triangles) and repulsive (circles). (c) $C_V$, reflecting (triangles) and repulsive (circles).

The bulk 3D and 2D limits of $\Delta$, shown in Fig. 1(a), are evaluated from the bulk simulations of a 3D fluid and 2D disks, respectively, at the same $\mu$ and $T$. Figure 1(a) shows $\Delta$ as a function of $H$ for reflecting and repulsive walls. $\Delta$ exhibits a clear 3D to 2D crossover in the case of reflecting walls: A steep rise in $\Delta$ takes place around a critical separation $H_c = 4\sigma$, where the structural crossover takes place in the central region as well. A similar crossover is observed for the repulsive walls also. The intimate connection of crossover in $\Delta$ and the structural changes at the central region is illustrated in Fig. 1(b), showing the behavior of $\Delta$ calculated over the central regions. The striking similarity of these plots with those in Fig. 1(a) confirms that the central fluid layer holds the key to this crossover. The constant volume specific heat [12,24] $C_V$ as a function of $H$ are featureless for both kind of walls [Fig. 1(c)], ruling out any thermodynamic phase transition associated with the crossover. This crossover in $\Delta$ qualitatively matches the sudden increase in fluctuations in the refractive index of cyclohexane confined between solvophobic mica plates with a separation just below 2 nm ($\sim H_c$), measured from surface force experiments [9]. Thus, $H_c$ matches with the length scale at which the jumps in $\tau$, $\varepsilon_0$, $\eta$, $D$, and $n$ are observed in experiments [4,7–9].

The crossover in $\Delta$ around $H_c$ can be made more explicit within a simple theoretical treatment focusing on the long-wavelength cutoff due to the confinement. $\Delta$ is given by the long-wavelength ($k\sigma \approx 0$) limit of the static structure factor $S(k\sigma)$ in bulk [25]. $S(k\sigma)$ can be calculated from the liquid direct correlation function $c(r)$ via the Ornstein-Zernike (OZ)

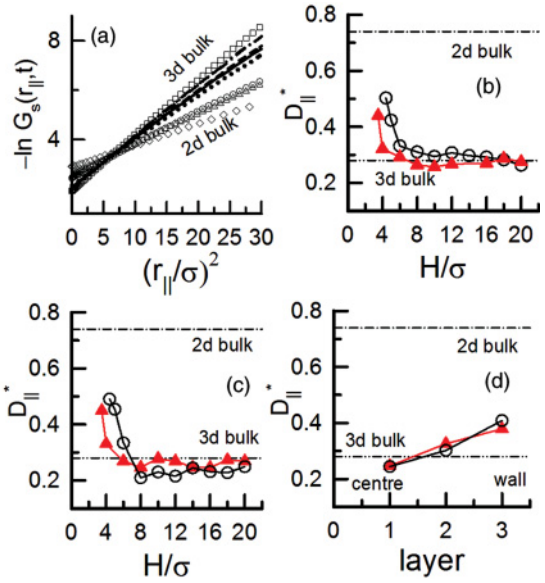


FIG. 2. (Color online) (a) Long-time limit of $-\ln G_s(r_\parallel,t)$ vs $r_\parallel^2$ in reflecting slits for $H = 3.5\sigma$ (triangles), $4\sigma$ (circles), $6\sigma$ (dotted), $8\sigma$ (solid), $10\sigma$ (dashed), $16\sigma$ (dashed-dotted), and $20\sigma$ (dashed-dotted-dotted) along with the corresponding 2D (diamonds) and 3D (squares) limits. (b) $D^*_\parallel$ for reflecting (triangles) and repulsive (circles) slits. (c) $D^*_\parallel$ of only the central region in a slit with reflecting (triangles) and repulsive (circles) walls. (d) Layerwise value of $D^*_\parallel$ in a slit of $H = 14\sigma$ with reflecting (triangles) and repulsive (circles) walls. The leftmost layer is the central region and the rightmost one is for the wall-adjacent layer. The middle one is for a layer in between the two.

relation [25]. Within mean-field approximations for LJ fluids, the $c(r)$ is split into correlations due to the short-ranged hard core, given by the Percus-Yevick form [25] $C^{\rm PY}(r)$ for $r < \sigma$ and an attractive tail, $C^{\rm LR}(r) = -4(\varepsilon/k_BT)(\sigma/r)^6$ for $r \geqslant \sigma$ [25]. In a slit geometry, we integrate over $\vec{r}_\parallel$ in $c(r)$ to yield $c(z)$. We compute $S(k_z\sigma)$, $k_z$ being the transverse component of a wave vector, using the OZ relation $S(k_z\sigma) = [1 - \rho c(k_z\sigma)]^{-1}$, where $\rho$ is the average fluid density in the slit obtained from GCMC simulations. We ignore the density inhomogeneity near the walls which is a good approximation here, since the homogeneous central region, showing the crossover, encompasses the majority of the slit. The spatial integration for the Fourier transform of $c(z)$ to calculate $c(k_z\sigma)$ becomes restricted as $z$ runs from zero to $H/2$ corresponding to a minimum wave vector $k_z^{\rm min}\sigma = 2\pi/H$. Here, $\Delta$ is defined by the value of $S(k_z^{\rm min}\sigma)$. A comparison of simulation and theoretical results for reflecting walls [Fig. 1(a)] reveals nearly quantitative agreement. This indicates that the crossover is a manifestation of cutoff in long-wavelength density fluctuations due to a geometrical constraint. The repulsive slit results also show good qualitative agreement between simulations and the theoretical estimate [Fig. 1(a)]. This is because the fluid layers in this case are formed away from the walls due to their repulsive nature, creating a geometrical constraint similar to reflecting walls.

The crossover shows up in the dynamic density fluctuations as well, as demonstrated in Fig. 2(a) by the long time ($t \sim 100$ times larger than the diffusion time scale required for a tagged particle to traverse the length of its diameter) behavior of $-\ln G_s(r_\parallel,t)$ as a function of $r_\parallel^2$ for different values of $H$. The plots, shown for the reflecting slits, are straight lines with slopes changing from 2D to 3D limit with a sudden change above $H = 4\sigma$. Note that the crossover in $D^*_\parallel (= D_\parallel[m/\sigma^2\varepsilon]^{1/2})$ almost coincides with that in $\Delta$. $D^*_\parallel$, for both the reflecting and repulsive walls [Fig. 2(b)], become maximum at the smallest value of $H$ and drops around $H = 6\sigma$ to meet the bulk 3D value. Physically, under maximum confinement, there is only one fluid layer resembling 2D fluid where the self-diffusion is faster compared to the 3D situation. The in-plane diffusivity drops, as the confinement is relaxed to accommodate multiple fluid layers, due to contributions from interlayer diffusion. Figure 2(c) shows $D^*_\parallel$ for the central layer, which indicates that the crossover in $D^*_\parallel$ is primarily due to the central region. Similar faster diffusion than bulk has been observed for cyclohexane in mica pores of a few nm width from NMR measurements [31], for water in carbon nanotubes using flow measurements [32] and in earlier simulations [33]. This trend, however, is absent in the shear viscosity data of water from atomic force microscopy (AFM) experiments with a hydrophobic graphite substrate [10]. This could be due to the fact that the geometry of a spherical tip sliding close to a planar solid does not represent the strong confinement limit.

We extract the in-plane diffusion coefficient for different layers as well. In Fig. 2(d) we show the $D^*_\parallel$ data for different layers for a reflecting and repulsive slit with $H = 14\sigma$. There are only three different layers present in the slits with these walls: the central region, the wall-adjacent layer and the layer in between. Nearly 3D bulklike diffusion is observed in the central region. The relatively faster in-plane diffusion observed in the wall-adjacent layer compared to the other layers is

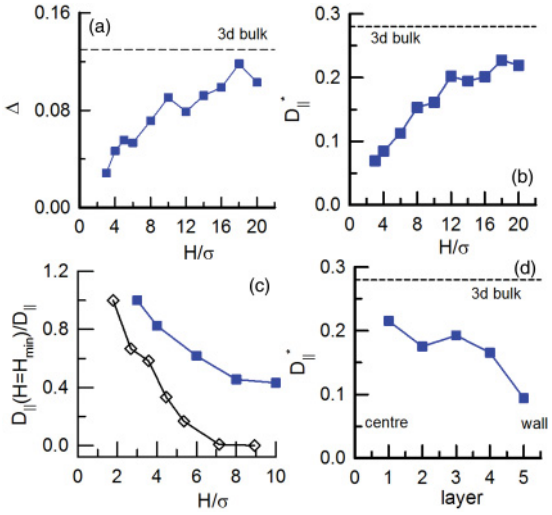


FIG. 3. (Color online) Different variables for the attractive slits as functions of $H$: (a) $\Delta$, (b) $D^*_\parallel$, and (c) calculated $D^*_\parallel(H_{\rm min})/D^*_\parallel(H)$ (squares) with a similar quantity $\eta(H)/\eta(H_{\rm min})$ for confined water (diamonds) [10]. (d) Layerwise value of $D^*_\parallel$ in a slit of $H = 14\sigma$ with attractive walls. The leftmost layer is the central region and the rightmost one is for the wall-adjacent layer. The data in between are for the middle layers.

probably due to the fact that, unlike other layers, the particles in this layer are in contact with the smooth wall in one side which makes the particles move faster compared to those which are in between two layers of particles.

Let us now consider the effect of different wall-particle interaction on the crossover. The case of the attractive walls is different compared to the reflecting and repulsive walls. Due to the attractive nature of the walls, the density in the fluid layers close to the wall becomes very high. This suppresses the fluctuation in the system which is reflected in very low values of $\Delta$ in the extreme confinement limit ($H \sim 3\sigma$) far from the bulk 2D value [Fig. 3(a)]. Unlike the reflecting and repulsive slits, here $\Delta$ gradually approaches the 3D limit for large $H$ from low values. The dependence of $\Delta$ on $H$ [Fig. 3(a)] agrees qualitatively with the observed trends in $\varepsilon_0$ for the water pool confined inside hydrophilic cavities of reverse micelles [7]. Under the strong confinements, $D_{\parallel}^{*}$ is about ten times smaller for the attractive slit [Fig. 3(b)] compared to those for the reflecting and repulsive walls. Variation of $D_{\parallel}^{*}$ is in agreement with the earlier simulation reports on water in hydrophilic silica pores [10,18]. Figure 3(c) shows the trends of the inverse of $D_{\parallel}^{*}$, qualitatively in agreement with the observations of the estimated viscosity ($\eta$) of water confined between an AFM tip and hydrophilic surfaces [10]. The layerwise diffusion is shown in Fig. 3(d) for $H = 14\sigma$. Note, here we get five distinct layers in total. $D_{\parallel}^{*}$ gradually decreases from the central to the wall-adjacent layer. The diffusivity in the central region is near the 3D bulk value while the particles in the high-density layer close to the wall are almost immobilized due to the attractive wall-fluid potential resulting in almost zero diffusivity.

In conclusion, we have shown that the dimensional crossover in static density fluctuations for a confined fluid can be understood from the modifications in the long-wavelength response of the fluid due to confinement-induced geometrical constraints. The dynamic density fluctuations also show the signature of this crossover. Our results provide a clear relation between the crossover of different physical properties and the length scale of confinement, although the detailed nature of the crossover is sensitive to the confining potential. Thus, we suggest a possible general mechanism for the crossover in a large number of diverse static and long-time dynamical quantities under confinement.

A.D. thanks the Council of Scientific and Industrial Research, India for support through a research fellowship. We thank P. Pradhan for useful comments and discussions.

[1] K. Bhattacharyya, Chem. Commun. **2008**, 2848 (2008).
[2] B. Bhushan, J. N. Israelachvilli, and U. Landman, Nature (London) **374**, 607 (1995).
[3] S. Granick, S. C. Bae, S. Kumar, and C. Yu, Physics **3**, 73 (2010).
[4] S. H. Khan, G. Matei, S. Patil, and P. M. Hoffmann, Phys. Rev. Lett. **105**, 106101 (2010).
[5] M. Erko, N. Cade, A. G. Michette, G. H. Findenegg, and O. Paris, Phys. Rev. B **84**, 104205 (2011).
[6] N. E. Levinger, Science **298**, 1722 (2002).
[7] R. Biswas, N. Rohman, T. Pradhan, and R. Buchner, J. Phys. Chem. B **112**, 9379 (2008).
[8] T.-S. Kim and R. H. Dauskardt, Nano Lett. **10**, 1955 (2010).
[9] M. Heuberger, M. Zach, and N. D. Spencer, Science **292**, 905 (2001).
[10] T.-D. Li, J. Gao, R. Szoszkiewicz, U. Landman, and E. Riedo, Phys. Rev. B **75**, 115415 (2007).
[11] M. Schoen, D. J. Diestler, and J. H. Cushman, J. Chem. Phys. **87**, 5464 (1987).
[12] M. P. Allen and D. J. Tildsley, *Computer Simulation of Liquids* (Clarendon, Oxford, UK, 1987).
[13] B. Götzelmann and S. Dietrich, Phys. Rev. E **55**, 2994 (1997).
[14] P. Bryk, W. Rżysko, A. Malijevsky, and S. Sokołowski, J. Colloid Interface Sci. **313**, 41 (2007).
[15] A. V. Neimark, P. I. Ravikovitch, and A. Vishnyakov, Phys. Rev. E **62**, R1493 (2000).
[16] S. Han, M. Y. Choi, P. Kumar, and H. E. Stanley, Nat. Phys. **6**, 685 (2010).
[17] M. Schoen, J. H. Cushman, D. J. Diestler, and C. L. Rhykerd Jr., J. Chem. Phys. **88**, 1394 (1988).
[18] S. R.-V. Castrillón, N. Giovambattista, I. A. Aksay, and P. G. Debenedetti, J. Phys. Chem. B **113**, 7973 (2009).
[19] T. Fehr and H. Lowen, Phys. Rev. E **52**, 4016 (1995).
[20] Y. Liu, A. Z. Panagiotopoulos, and P. G. Debenedetti, J. Chem. Phys. **132**, 144107 (2010).
[21] S. K. Singh, J. K. Singh, S. K. Kwak, and G. Deo, Chem. Phys. Lett. **494**, 182 (2010).
[22] R. L. C. Vink, K. Binder, and J. Horbach, Phys. Rev. E **73**, 056118 (2006).
[23] For instance, $\varepsilon_0$ of a dipolar fluid of bulk density $\rho$ is related to the long-wavelength limit of the dipole moment density $\boldsymbol{M}(\mathbf{k})$ of the system [25], $(\varepsilon_0 - 1)(2\varepsilon_0 + 1)/\varepsilon_0 = 4\pi\rho L t_{k\sigma\to 0}\langle \boldsymbol{M}_{\mathbf{k}}\boldsymbol{M}_{-\mathbf{k}}\rangle/Nk_BT$, where $k_B$ is the Boltzmann constant. Now, $\boldsymbol{M}(\mathbf{k}) \propto \rho(\mathbf{k})$, the Fourier component of the microscopic fluid density, hence connects $\varepsilon_0$ with the long-wavelength limit of density fluctuation. The refractive index $n = \sqrt{\varepsilon_0}$ thereby is related to density fluctuations.
[24] D. J. Adams, Mol. Phys. **29**, 307 (1975).
[25] J. P. Hansen and I. R. McDonald, *Theory of Simple Liquids*, 3rd ed. (Academic, San Diego, 2006).
[26] We calculate the $T$ from fluctuations of kinetic energy and $\mu$ by inserting test particles [12]. The mean values of the $T$ and $\mu$ agree to those of the GCMC simulations. We have checked that these quantities remain similar for different initial conditions chosen from equilibrated GCMC configurations.
[27] N. B. Wilding, Am. J. Phys. **69**, 1147 (2001).
[28] S. Dietrich and A. Haase, Phys. Rep. **260**, 1 (1995).
[29] The in-plane 2D RDF [11,28] is defined as $g(r_{\parallel}) = \langle N(r_{\parallel})/2\pi r_{\parallel}\Delta r_{\parallel}\rho_{2D}^{l}(z)n_l\rangle$ for a layer at $z$ of width $\Delta z$ ($\leqslant\sigma$) with $n_l$ particles, where $r_{\parallel} = \sqrt{x^2 + y^2}$, and layer density $\rho_{2D}^{l}(z) = n_l/A$, where $A$ is the cross-sectional area of the slit along the

$xy$ direction. For a wider layer ($\Delta z \geqslant \sigma$), we compute the 3D $g(r) = \langle N(r)/4\pi r^2 \Delta r \rho_{3D}^{l} n_l \rangle$, where $r = \sqrt{x^2 + y^2 + z^2}$, and layer density $\rho_{3D}^{l} = n_l / A\Delta z$.

[30] N. E. Levinger and L. A. Swafford, Annu. Rev. Phys. Chem. **60**, 385 (2009).

[31] S. Stapf, R. Kimmich, and T. Zavada, Appl. Magn. Reson. **12**, 199 (1997).

[32] J. K. Holt *et al.*, Science **312**, 1034 (2006).

[33] O. Beckstein and M. S. P. Sansom, Proc. Natl. Acad. Sci. USA **100**, 7063 (2003).